NUCL SCI TECH (2019) 30:130
https://doi.org/10.1007/s41365-019-0653-8

A study of PFBR auxiliary neutron source strength activation and its variability with respect to the neutron spectrum and ^{123}Sb capture cross section

G. Pandikumar[1] · D. Sunil Kumar[1] · M. M. Shanthi[1] · Bagchi Subhrojit[1] · A. John Arul[1] · D. Venkata Subramanian[1] · Rajeev Ranjan Prasad[1]

Received: 23 July 2018 / Revised: 22 February 2019 / Accepted: 6 April 2019 / Published online: 22 July 2019

Abstract In fast reactors, the inherent neutron source strength is often insufficient for monitoring the reactor start-up operation with ex-core detectors. To increase the subcritical neutron flux, an auxiliary neutron source subassembly (SSA) is generally used to overcome this problem. In this study, the estimated neutron source strength and detector count rate of an antimony–beryllium-based SSA are obtained using the deterministic transport code DORT and Monte Carlo calculations. Because the antimony activation rate is a critical parameter, its sensitivity to the capture cross section and neutron flux spectrum is studied. The reaction cross section sensitivity is studied by considering data from different evaluated nuclear data files. It is observed that, because of the variation in the cross sections from different evaluated nuclear data files, the values of the saturation gamma (> 1.67 MeV) activity and neutron strength predicted by ORIGEN2 lie within ± 2%. The obtained antimony activation rate and sensitivity to the neutron flux are partially validated by irradiating samples of antimony in the KAMINI reactor. The average one-group capture cross sections of bare and cadmium-covered ^{123}Sb samples obtained by the ratio method are 4.0 and 1.78b, respectively. The results of the calculation predicting the activated neutron source strength as a function of operating time and sensitivity to the neutron spectrum in the irradiation region are also presented.

Keywords Fast reactors · Neutron source · Core monitoring · Neutron and gamma transport · Antimony activation · Material depletion

1 Introduction

In the Prototype Fast Breeder Reactor (PFBR), the status of the core during regular start-ups as well as during reactor shutdown is monitored by high-temperature fission counters (HTFCs) with a sensitivity of 0.2 cps/nv, which are located in the control plug above the core [1]. However, it is found that the inherent neutron source strength arising from spontaneous fission and (α, n) reactions with oxygen nuclei in the fuel is insufficient to provide an acceptable count rate for core monitoring. Therefore, auxiliary neutron source subassemblies (SSAs) are planned to provide a count rate of more than 3 cps, as required owing to safety and start-up time considerations [1]. The SSA consists of antimony (Sb_2O_3) pin bundles placed in hexagonal beryllium blocks. Neutrons are produced by the threshold (1.67 MeV) photoneutron reactions in beryllium. An antimony–beryllium photoneutron source is selected owing to its ease of fabrication and handling before loading into the reactor and its capacity for regeneration during operation. The SSA is located at the interface of the core periphery and radial blanket.

The neutron and gamma source strengths were estimated using the two-dimensional (2D) neutron transport code DORT [2]. The correctness of the neutron source strength estimate depends on the antimony activation calculation, which in turn depends on the neutron flux and ^{123}Sb capture cross section. Hence, in addition to the estimation of

✉ G. Pandikumar
pkg@igcar.gov.in

1 Reactor Shielding and Data Division, Department of Atomic Energy, Nuclear Systems Design Group, Reactor Design Group, Indira Gandhi Centre for Atomic Research, Kalpakkam 603102, India

the neutron source strength and detector count rates, sensitivity and partial validation studies are performed.

The results are partially validated, and the sensitivity to the thermal neutron flux is determined by irradiating samples of antimony in the KAMINI [3] reactor. Samples of (1) bare antimony and gold and (2) antimony and gold covered with cadmium to cut off the thermal flux are irradiated. From these experiments, the neutron-flux-spectrum-averaged one-group capture cross sections of the bare and cadmium-covered ^{123}Sb samples are obtained by the ratio method. The change in the one-group cross section indicates the effect of spectral modification.

The sensitivity and variability of saturated gamma activity with respect to the antimony capture cross section are studied by considering data from various evaluated nuclear data files (ENDFs). An ENDF presents the best cross sections from both experiments and theoretical predictions. However, such ENDFs, for example, ENDF/B-VII.1 [4], JENDL-4.0 [5], and ROSFOND [6], are produced by different groups of evaluators. Owing to differences in the experimentally obtained and theoretically predicted data considered by the evaluators, the cross section data can vary.

This paper is organized as follows: Sect. 2 describes core monitoring by means of neutron detectors in the PFBR in detail. Section 3 gives the geometrical details of the auxiliary SSA and the data required for modeling. Section 4 covers the calculation of the neutron source strength from the SSA and the count rate at the control plug detector locations. The variation in the source strength with burnup owing to antimony depletion and decay is also presented. Section 5 discusses the experimental validation of the ^{123}Sb capture rate. In Sect. 6, the source strength variability with respect to the neutron spectrum in the antimony resonance capture region and the capture cross sections from different data libraries are presented.

2 PFBR core monitoring

The PFBR is a 500 MWe, sodium-cooled, pool-type, mixed-oxide-fueled demonstration fast breeder reactor under construction at Kalpakkam [7]. The active core consists of 181 fuel subassemblies with two fissile enrichment zones of PuO_2. The core is enveloped by a blanket, which is surrounded by neutron reflector and shield assemblies.

The initial core loading and first approach to criticality will be monitored by three HTFCs with a sensitivity of 0.1 cps/nv, which will be located in a special central subassembly called the instrumented central subassembly [1]. However, for routine start-up of the reactor, the core will be monitored by HTFCs with a sensitivity of 0.2 cps/nv located in the control plug above the core. Because the inherent neutron source strength is insufficient to provide an acceptable count rate of more than 3.0 cps, antimony–beryllium-based auxiliary neutron SSAs will be used to provide enough source strength that start-up operations can be performed safely.

3 SSA geometry and properties

The auxiliary SSA is located at the core–blanket interface (eighth ring), as shown in Fig. 1. Three possible locations for the SSA are indicated. The auxiliary SSA consists of an antimony pin bundle enveloped by a hexagonal beryllium block. The bundle has 61 pins of Sb_2O_3 arranged in a hexagonal array. Each pin has ten capsules of Sb_2O_3 stacked inside a stainless steel tube, as shown in Fig. 2. The length of each capsule is 4.4 cm. The theoretical density of Sb_2O_3 is 5.2 g/cc. The pellet density is 90% of the theoretical density, and the mass of antimony oxide is 1.88 kg. The length, mass, and density of the beryllium block are 57 cm, 6.0 kg, and 1.66 g/cc, respectively. The dimensional details and a cross-sectional (*X*–*Y*) view of the SSA are shown in Fig. 3.

Antimony has two isotopes, ^{121}Sb and ^{123}Sb, which have isotopic abundances of 57.36% and 42.64%, respectively. Neutron interaction in ^{123}Sb results in production of ^{124}Sb, which has a half-life of 60.9 days. Beta decay of ^{124}Sb results in the production of ^{124}Te in an excited state. The decay scheme of ^{124}Te includes approximately 70 gamma transitions with energies between 148 and 2807 keV. Emission of neutrons from beryllium requires gamma rays with energies greater than 1.67 MeV. Therefore, the

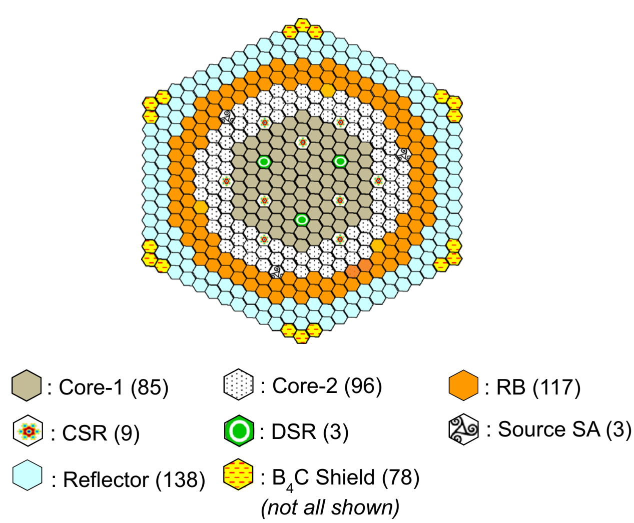

Fig. 1 Core configuration of PFBR. (Numbers in parentheses represent total number of SAs in each region.) (Color online)

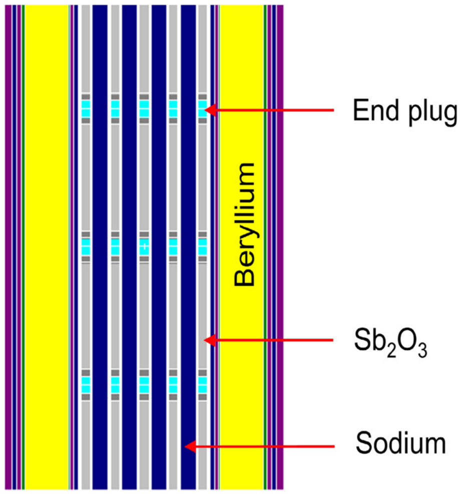

Fig. 2 (Color online) Sb_2O_3 pin bundle

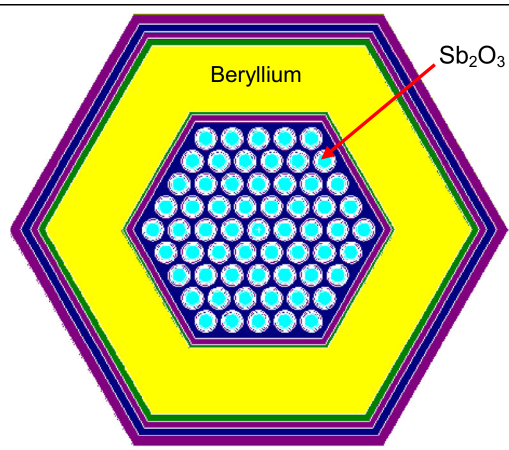

Be block	A/F 11.2/7.2 cm
Thickness of Be	2 cm
Sb_2O_3pellet radius	0.218 cm
Sb_2O_3pellet length	4.4 cm
No. of pins	61
Capsule tube inner/outer radii	0.218/0.255 cm
Clad inner/outer radii	0.285/0.33 cm

Fig. 3 Cross-sectional view of PFBR auxiliary SSA

1.69 MeV (yield 49%) and 2.1 MeV (yield 5.7%) gamma rays from ^{124}Te contribute to the photoneutron production.

4 Source strength estimation

The following four calculation steps are used to estimate the SSA neutron source strength and detector count rate for modeling convenience:

1. Estimation of activation of ^{123}Sb to ^{124}Sb by neutron flux in the SSA location
2. Estimation of gamma transport in beryllium and photoneutron yield
3. Modeling of neutron transport from SSA to control plug detector location
4. Shutdown count rate estimation

4.1 ^{123}Sb activation calculation

To determine the saturated gamma strength of the antimony pins, the neutron flux distribution in the antimony region in the SSA is required. The neutron distribution reaching the SSA (which is kept in the first row of the blanket) is estimated using a 2DRZ model of the PFBR core and radial blanket without the SSA, as shown in Fig. 4a. To this end, a neutron flux calculation is performed using the deterministic 2D neutron and gamma transport code DORT and the IGC-S3 cross section set. IGC-S3 is a

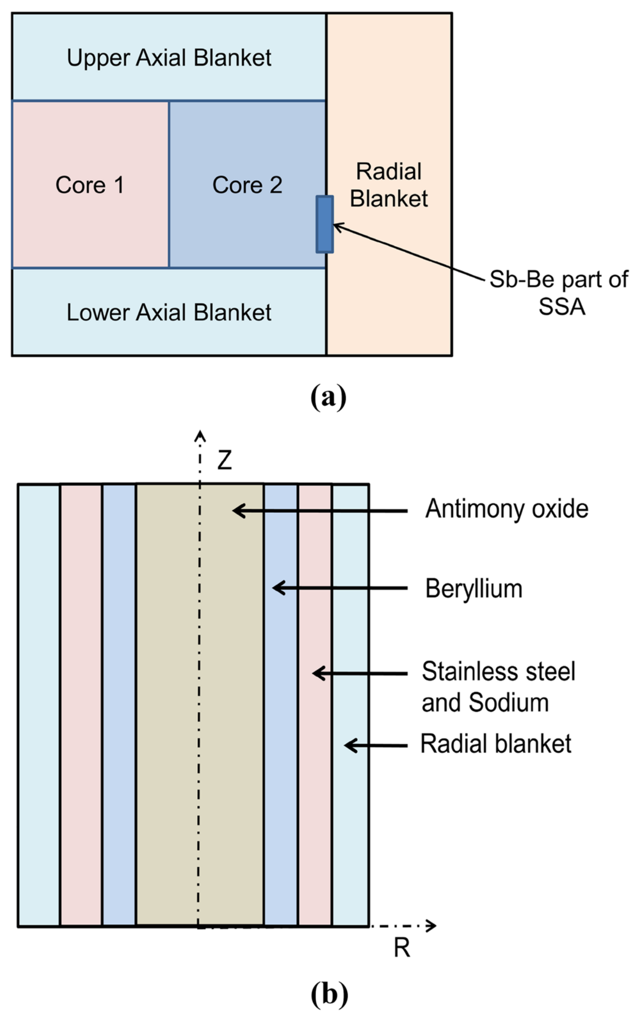

Fig. 4 (Color online) RZ model of PFBR (**a**) and SSA (**b**)

coupled neutron–gamma cross section set having 175 neutron and 42 gamma group structures, which was prepared from ENDF/B-VI.8 [8, 9]. The neutron flux in the outer core and blanket region is approximately 3.10×10^{15} n/cm^2/s. Then, to obtain the average neutron flux in the antimony region, the neutron spectrum in the core blanket region obtained from this calculation is distributed in the antimony region, which is shown in the model in Fig. 4b, and an additional transport calculation is performed.

The number of gammas emitted from the antimony region is computed using the average neutron flux spectrum in the antimony region and the capture cross section of ^{123}Sb. At full power, the average neutron flux in the antimony region is found to be 2.66×10^{15} n/cm^2/s. The estimated total ^{123}Sb capture reaction rate per SSA is 9.04×10^{15} s^{-1}.

4.2 Gamma transport and photoneutron yield estimation

To obtain the average gamma flux in the beryllium region, the gamma transport is calculated using the RZ geometry shown in Fig. 4b. In this case, the gamma flux estimated in the antimony region is used as the distributed source. The gamma flux transported from the antimony region to the beryllium region is extracted. From this, the estimated saturation gamma strength in the beryllium region (> 1.67 MeV) is 4.95×10^{15} γ/s/SA.

Using the same total neutron flux of 2.66×10^{15} n/cm^2/s, the saturation gamma activity for 300 days of irradiation is also estimated using the versatile isotope buildup code ORIGEN2 [10]. The estimated saturation gamma strength (> 1.6 MeV) from an SSA is approximately 4.75×10^{15} γ/s. It is observed that the saturation gamma strength predicted by DORT is approximately 4% higher than that predicted by ORIGEN2.

Then, the total photoneutron reaction rate is estimated using the average saturation gamma flux in beryllium and the beryllium photoneutron cross section from ENDF/B-VII.1. The neutron source strength calculated by this method is 9.26×10^{11} n/s/SA (saturated), and the estimated neutron yield is 1.87×10^{-4} n/γ. The photoneutron yield is also verified by an independent application-specific Monte Carlo simulation (MCS) of gamma transport in the SSA by assuming a uniform gamma source strength in the antimony pins and subsequent transport through the pins and beryllium block. The photonuclear and photoatomic interaction cross sections are obtained from ENDF/B-VII.1. Table 1 gives the estimated neutron yield per gamma. The results show that the neutron yields per gamma for the SSA antimony–beryllium geometry obtained by the two methods are in very good agreement.

4.3 Neutron transport from SSA to control plug detector location

After the neutron strength from the SSA is determined, the transport of neutrons from the SSA in the core to the control plug detector location is modeled by MCNP-4B [11]. Figure 5a shows a schematic diagram of the active core and detector location. The initial plan, considering uncertainties and operational convenience, is to have three SSAs at the core–blanket interface (see Fig. 1). These three SSAs are included in the beginning-of-life core and can be replaced in turn after the third, fourth, and fifth cycles of operation. There are three HTFCs located 14.8 cm vertically above the core SA head and 100 cm radially from the core center (Fig. 5b). The detector active height is 27 cm. The model consists of three SSAs and three detectors in the control plug location. In the calculation, it is assumed that the saturated neutron strength of 9.26×10^{11} n/s/SA is distributed uniformly in each SSA region. Further, 10^9 particle histories with the F4 tally were employed for the calculation.

4.4 Estimation of shutdown count rates

From the neutron flux calculated at the detector location in the previous step, the ^{235}U thermal fission equivalent flux is calculated using the following expression:

$$\emptyset_{\text{fis-eq}} = \frac{\int \emptyset(E)\sigma_f^{\text{u}-235}(E)\text{d}E}{\sigma_f^{\text{u}-235}(0.025\ \text{eV})}. \tag{1}$$

The thermal cross section of ^{235}U fission is 585.1b. Hence, the total detector counts are calculated by multiplying the fission equivalent flux by the detector sensitivity. For the three SSAs inside the core, with an HTFC sensitivity of 0.2 cps/nv at the control plug location, the count rates estimated in the three detectors are 35.1, 38.4, and 38.6 cps, respectively. Further, the count rates from the three detectors with one SSA are 13.0, 13.8, and 14.0 cps, respectively. The small differences in the count rates are due to the asymmetry of the detector location (Fig. 5b).

The saturation source strength of the auxiliary SSA decreases during reactor operation owing to burnup of antimony. Figure 6 shows the activity buildup and decay of ^{124}Sb during each cycle of operation. It is assumed that each fuel cycle consists of 6 months of full-power operation followed by 2 months of shutdown for fuel handling. When the reactor is operating at full power, the source strength of the auxiliary SSA builds up from zero, and it increases to approximately 50% of saturation in 2 months. After 6 months of full-power operation, it reaches 88% of saturation at the end of the first cycle (EOC1). After 2 months of reactor shutdown, the ^{124}Sb activity decreases to 44% of saturation.

Table 1 Neutron yield per gamma from MCS

Code	Gamma flux in Be (γ/cm^2/s) 1.69–1.7 (MeV)	Neutron yield (n/$\gamma > E_{th}$)	Remarks
DORT	3.13×10^{-4}	1.87×10^{-4}	Gamma rays with energies > 1.69 MeV were considered
Application-specific MCS	3.20×10^{-4}	1.81×10^{-4}	2.1 MeV gamma rays were neglected

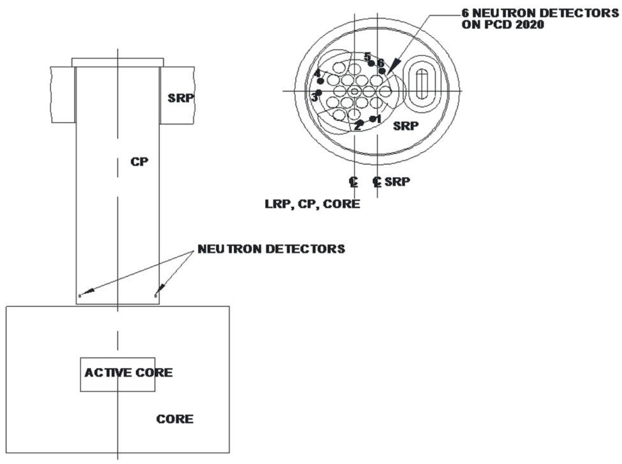

(a)

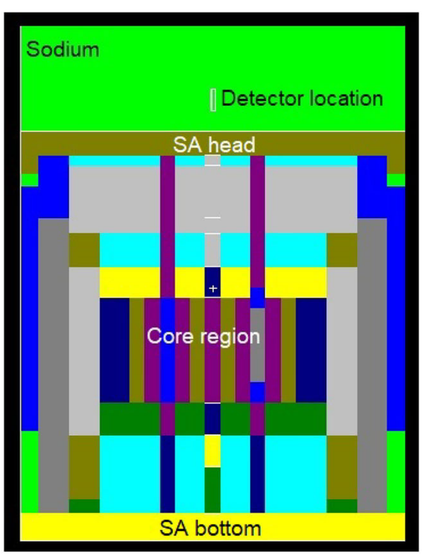

(b)

Fig. 5 (Color online) **a** Schematic of control plug detector location (*LRP* large rotating plug, *SRP* small rotating plug, *CP* control plug, *PCD* pitch-to-center distance); **b** vertical cross-sectional view of MCNP model of PFBR core up to control plug. (A horizontal cross-sectional view of the PFBR core is shown in Fig. 1.)

Note that gammas produced by the core with energies above the threshold energy (1.69 MeV) will also result in neutron generation from the SSA. During full-power

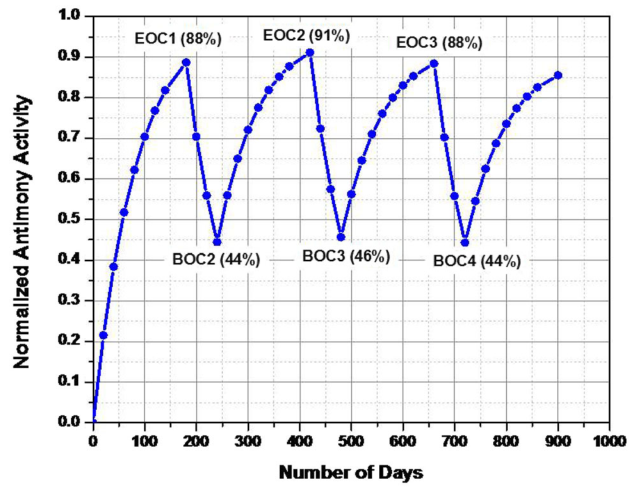

Fig. 6 Antimony activity during each cycle of operation

operation, the neutron source strength is approximately 5.56×10^{12} n/s, which is six times larger than the neutron source strength from the SSA. However, after approximately 2 months of shutdown, the neutron source strength from the core gammas is 1.58×10^{10} n/s, which is 26 times smaller than that from an SSA.

Figure 7 shows the neutron strengths and count rates corresponding to saturation, EOC1, and 1 and 2 months after reactor shutdown. These count rates also include contributions from the inherent neutron source (INS). The INS contributions are estimated using the homemade code NSOURCE. The estimated count rates resulting from INSs at the end of one cycle, 1 month after shutdown, and 2 months after shutdown are 0.6, 0.54, and 0.49 cps, respectively.

5 Experimental validation of antimony activation

Experimental studies are performed by irradiating samples of antimony in the KAMINI reactor. Samples of (1) bare antimony (powder) and gold and (2) antimony (powder) and gold covered with cadmium to filter the thermal flux are irradiated. The samples are irradiated separately for each case. Each sample is inserted adjacent to the core of KAMINI using the Pneumatic Fast Transit

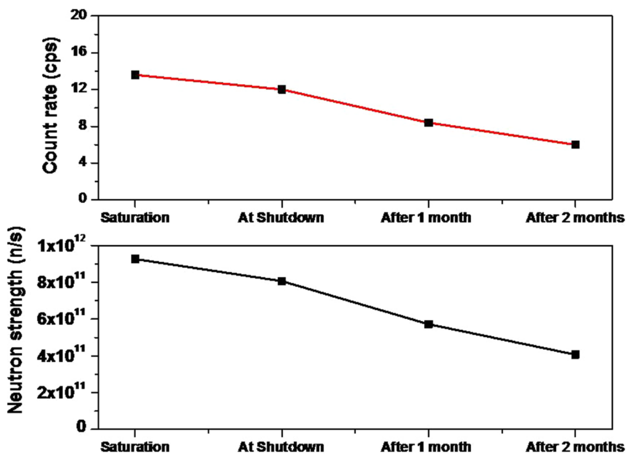

Fig. 7 Count rate and neutron strength corresponding to saturation, shutdown, and 1 and 2 months after reactor shutdown

System (PFTS). Cadmium-covered foils are used to analyze the epithermal neutron activation, as the KAMINI spectrum is soft compared to that at the SSA location in the PFBR. Irradiation of gold foils serves as a reference for finding the activation cross section of antimony through the activity ratio method.

The reactor was operated at 10 kW. The four samples, i.e., bare gold, bare antimony, cadmium-covered gold, and cadmium-covered antimony, were irradiated separately for 600 s each. The irradiated samples were measured using an HPGe detector at a reference position with a known full-energy peak detection efficiency. The detector has a 30% relative efficiency, and the resolution was 2.0 keV at the 1332 keV peak of ^{60}Co. The peak areas were evaluated using the peak fitting software APTECH. The details of the foils (powder) and their measured reaction rate and measured activities are given in Table 2. The measured reaction rate (R) is obtained as:

$$R = \frac{C_{\text{peak}}\lambda}{Ny\varepsilon \mathrm{e}^{-\lambda T_{\mathrm{d}}}[1-\mathrm{e}^{-\lambda T_{\mathrm{c}}}][1-\mathrm{e}^{-\lambda T_{\mathrm{irr}}}]}, \quad (2)$$

where C_{peak} is the net peak area of the full-energy photopeak measured by the HPGe detector, y is the gamma intensity (gammas/decay), ε is the efficiency of the detector, T_{d} (s) is the time delay between the end of irradiation and the start of counting, T_{c} is the counting time (s), T_{irr} is the irradiation time, and N is the number of target atoms in the foil. The efficiency of the HPGe detector was obtained as a function of gamma ray energy using a ^{152}Eu standard.

The activation (average) cross section of gold is obtained as:

$$\sigma_2 = \frac{R_2}{\phi}, \quad (3)$$

where σ_2 and R_2 represent the KAMINI spectrum-averaged capture cross section and measured reaction rate of gold, respectively. The KAMINI PFTS neutron flux spectrum, ϕ, is measured using the foil activation technique and unfolded in 175 neutron groups [12] in these calculations. The unfolding method utilizes ten activation reactions (activation foils) to cover the energy range of 1.0×10^{-4} eV to 20 MeV. Although the error of the unfolded neutron flux has not been estimated, it is reported that the unfolded spectrum reproduces the measured reaction rates within a $\pm$ 10% error [12]. Then, using the ratio method as described below, the average one-group capture cross section of ^{123}Sb can be obtained if an accurate cross section of the reference sample (gold) is known.

$$\frac{A_1}{A_2} = \frac{N_1\sigma_1\phi}{N_2\sigma_2\phi}, \quad (4)$$

where A_1 and A_2 are the activities of ^{123}Sb and ^{197}Au (Bq), and N_1 and N_2 are the number of atoms of ^{123}Sb and ^{197}Au, respectively; σ_1 represents the average capture cross section of ^{123}Sb. The cadmium-covered samples are sandwiched between cadmium foils. The presence of cadmium reduces not only the thermal component, but also the total neutron strength. The antimony is activated mainly by epithermal neutrons. The reduced neutron flux that

Table 2 Details of the foils and their measured reaction rate and activity

Foil/granule	Mass (mg)	Thickness (mm)	Measured reaction rate (per atom)	Measured activity (Bq)	Average cross section (b)
Au	13.4	0.04	3.01×10^{-11}	1.23×10^{9}	100.00
Sb	403.2	–	1.24×10^{-12}	1.05×10^{9}	4.10
Cd-covered Au					
Cd	413.6	0.27			
Au	203.6	0.20	3.95×10^{-12}	2.46×10^{9}	14.11
Cd-covered Sb					
Cd	392.8	0.27			
Sb	157.2	–	4.97×10^{-13}	1.64×10^{8}	1.78

activates the antimony or gold is approximated using the attenuation equation $\phi = \phi_o e^{-\Sigma_t t}$, where ϕ_o and ϕ are the incident and transmitted neutron fluxes, respectively, Σ_t is the macroscopic total cross section of cadmium, and t is the thickness of the cadmium foil. Then, following a methodology similar to that used for the bare samples, the average activation cross sections of the cadmium-covered gold and antimony samples are obtained. The measured activities and the cross sections obtained using Eq. (4) are given in Table 2. It is observed that, owing to the spectral change, the average capture cross section of ^{123}Sb decreases from 4.1 to 1.78b. The measured and calculated reaction rates for bare ^{123}Sb are 1.24×10^{-12} and 1.34×10^{-12} reactions/atom/s, respectively. The difference between the measured and calculated values is approximately 8%. The experimental study helped to validate the one-group cross section of ^{123}Sb and hence the ^{123}Sb activation with the nearest available spectrum from KAMINI. Further sensitivity studies are presented in the following sections.

6 Source strength variability and sensitivity studies

Section 4 discussed the theoretical predictions of the neutron and gamma source strength. There is sufficient confidence in the estimated flux at the SSA location and the spectrum estimates from integral experiments and fast breeder test reactor design and operation experience [13]. However, the estimated ^{123}Sb capture rate requires further assessment. In this context, the variability of the estimates with respect to the capture cross sections of ^{123}Sb from different evaluated cross section libraries is also assessed. The following subsections discuss (1) the prediction of the saturation gamma activity using ^{123}Sb capture cross sections from different ENDFs and (2) the sensitivity to the neutron spectrum in the region surrounding the SSA.

6.1 Source strength intercomparison with cross section data from different ENDFs

Since ORIGEN2 has been used in this study to estimate the saturated gamma activity, the geometry and material details are included in the calculation only through the reactor-dependent spectrum-averaged self-shielded one-group cross section, and the results could be sensitive to the one-group cross section. An ENDF which is used to prepare the one-group cross section has the best cross sections from both experiments and theoretical predictions. However, such ENDFs, for example, ENDF/B-VII.1 [4], JENDL-4.0 [5], and ROSFOND [6], are produced by different groups of evaluators. Owing to differences in the experimentally obtained and theoretically predicted data considered by the evaluators, the cross section data can vary. Therefore, to study the variability of saturated gamma activity with respect to the antimony capture cross section, gamma and neutron source strengths are estimated using ORIGEN2 with multi-group cross section data from ENDF/B-VII.1, JENDL-4.0, and ROSFOND. The neutron flux in the SSA location (surrounded by blankets) is used for the group collapsing.

The estimated one-group cross sections, ORIGEN2-predicted total gamma activity, neutron strengths, and percent deviation from their mean values are given in Table 3.

6.2 Sensitivity to spectrum in the region surrounding the SSA

Because antimony activation is very sensitive to the spectral component of the flux below 100 keV (which accounts for 80–90% of the reactions), the source strength was also estimated with the blanket SA replaced by a steel SA. In this case, the source strength increases by a factor of 3.9. (The ^{123}Sb capture reaction rate per atom for the steel-surrounded case is 2.72×10^{15} n/cm^2/s, and that for the blanket-surrounded case is 6.90×10^{14} n/cm^2/s.)

Figure 8 shows the absolute neutron flux spectra at the SSA location for the SSA surrounded by a blanket SA and

Table 3 Gamma and neutron source strength from different evaluations

Evaluation	σ_1^b (b)	Saturation gamma activity (γ/s/SA)				Neutron strength (n/s/SA)	
		Total	D^a (%)	>1.6 MeV	D^a (%)	>1.6 MeV	D^a (%)
ENDF/B-VII.1	1.137	2.87×10^{16}	0.95	4.83×10^{15}	1.5	9.04×10^{11}	1.7
JENDL-4.0	1.124	2.85×10^{16}	0.28	4.78×10^{15}	0.4	8.94×10^{11}	0.6
ROSFOND-2010	1.095	2.81×10^{16}	− 1.23	4.66×10^{15}	− 2.0	8.72×10^{11}	− 1.9
Average		2.85×10^{16}		4.75×10^{15}		8.89×10^{11}	

[a] D represents the deviation with respect to the average value

[b] σ_1 represents the spectrum-averaged one-group capture cross section

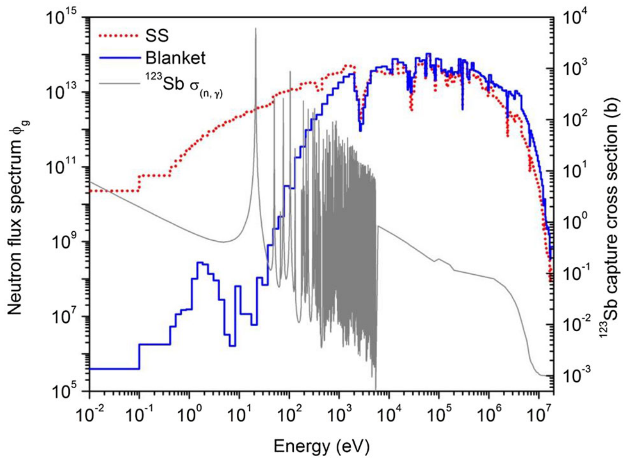

Fig. 8 (Color online) Neutron flux spectra at SSA location for blanket and steel SAs

the SSA surrounded by steel SA and the ^{123}Sb capture cross section. The spectral softening for the SSA surrounded by a steel SA is attributed to the fact that steel provides greater inelastic slowing down than the uranium oxide blanket material. The study indicates that the neutron source strength can be increased, if necessary, by the addition of a suitable steel SA surrounding the SSA, although this will reduce the breeding ratio.

The following are the salient observations from the studies of the auxiliary source strength activation, variability, and sensitivity.

1. The differences among the saturation gamma (> 1.67 MeV) activities and neutron strengths predicted by ORIGEN2 using one-group cross sections from different ENDFs are within ± 2%. In addition, the DORT estimate is approximately 4% higher than the ORIGEN2 prediction.
2. The source strength increases by a factor of 3.5 when the SSA is surrounded by a steel SA instead of a blanket SA owing to spectral softening.
3. An experimental study shows that the estimated one-group cross sections are sensitive to the flux spectrum in the thermal region. The estimated one-group antimony activation cross section in the KAMINI spectrum is 4.1b (11% at < 30 eV), whereas for the PFBR spectrum, it is 1.0b (1% at < 30 eV).

7 Conclusion

Using a combination of deterministic and Monte Carlo transport codes, the neutron source strength and control plug detector count rate from the auxiliary neutron SSA in the PFBR are estimated. The estimation is performed in four stages: (1) estimation of the ^{123}Sb activation using neutron flux in the SSA location, (2) estimation of gamma transport in beryllium and photoneutron yield, (3) modeling of neutron transport from SSA to control plug detector location, and (4) estimation of shutdown count rate. The estimated (saturated) neutron source strength of the SSA is approximately 9.3×10^{11} n/s/SA.

The accuracy of the neutron source strength estimate is sensitive to the neutron spectrum in the vicinity of the ^{123}Sb capture cross section resonance peak at 22 eV. Hence, the spectrum sensitivity is estimated by surrounding the SSA with a steel SA. The variability in the neutron source strength owing to the variation in the capture cross section is studied by considering data from different ENDFs. Experimental irradiation of antimony powder is also conducted and provides partial validation of the neutron source strength predictions in the absence of direct measurement of the PFBR spectrum.

Acknowledgements The authors are thankful to Mr. M. Thangamani, ENCO, KAMINI; Mr. D. Visweswaran, Mr. M. Elumalai, and Mr. N. Balakrishnan, Shift Engineers, KAMINI; Ms. R. Akila and Mr. D. Saravanan, Health Physicists, for their kind cooperation during sample irradiation at KAMINI; and Mr. Adish Haridas, RSDD, for his support of the gold and antimony activation experiments. The authors also thank the Director of RDG and Associate Director of NSDG for their constant encouragement and support.

References

1. M. Sivaramakrishna, C.P. Nagaraj, K. Madhusoodanan et al., Neutron flux monitoring system in prototype fast breeder reactor. IJEIT **3**(10), 45–53 (2014)
2. W.A. Rhoades, R.L. Childs, The DORT two-dimensional discrete ordinates transport code. Nucl. Sci. Eng. **99**, 88–89 (1988). https://doi.org/10.13182/NSE88-A23547
3. S. Usha, R.R. Ramanarayanan, P. Mohanakrishnan et al., Research reactor KAMINI. Nucl. Eng. Des. **236**, 872–880 (2006). https://doi.org/10.1016/j.nucengdes.2005.09.033
4. M.B. Chadwick, M. Herman, P. Oblozinsky et al., ENDF/B-VII.1: Nuclear Data for science and technology: cross sections, covariances, fission product yields and decay data. Nucl. Data Sheets **112**, 2887–2996 (2011). https://doi.org/10.1016/j.nds.2011.11.002
5. K. Shibata, O. Iwamoto, T. Nakagawa et al., JENDL-4.0: A new library for nuclear science and engineering. J. Nucl. Sci. Technol. **48**, 1–30 (2011). https://doi.org/10.1080/18811248.2011.9711675
6. A.I. Blokhin, A.V. Ignatyuk, V.N. Manokhin, et al., BROND-2.2, Russian evaluated neutron reaction data library, IAEA-NDS-90 Rev.8 (International Atomic Energy Agency, 1994)
7. S.C. Chetal, V. Balasubramaniyan, P. Chellapandi et al., The design of the prototype fast breeder reactor. Nucl. Eng. Des. **236**, 852–860 (2006). https://doi.org/10.1016/j.nucengdes.2005.09.025
8. K. Devan, G. Pandikumar, M. Alagan et al., Effects on the use of ENDF/B-VI neutron cross sections with anisotropy on the shield design of a pool type 500 MWe FBR. Ann. Nucl. Energy **30**, 1181–1197 (2003). https://doi.org/10.1016/S0306-4549(03)00040-9

9. P.F. Rose, ENDF-201–ENDF/B summary documentation, (ENDF/B-VI) BNL-NCS-17541, Brookhaven National Laboratory, NY, U.S.A., (1991), in *ENDF-102 Data Formats and Procedures for the Evaluated Nuclear Data File, ENDF-6, Brookhaven National Laboratory report BNL-NCS-44945 Rev. 2/97*, ed. by V. McLane, C.L. Dunford, P.F. Rose (1997)
10. A.G. Croff, ORIGEN2: A versatile computer code for calculating the nuclide composition and characteristics of nuclear materials. Nucl. Technol. **62**, 335–352 (1983). https://doi.org/10.13182/NT83-1
11. J.K. Shultis, R.E. Faw, *An MCNP primer*, Manhattan, KS 66506 (2011)
12. G.V.S. AshokKumar, S. Sujoy, E. Radha et al., Studies on neutron spectrum characterization for the pneumatic fast transfer system (PFTS) of KAMINI reactor. Appl. Radiat. Isot. **124**, 49–55 (2017). https://doi.org/10.1016/j.apradiso.2017.03.009
13. G. Srinivasan, K.V. Sureshkumar, B. Rajendran et al., The fast breeder test reactor—design and operating experiences. Nucl. Eng. Des. **236**, 796–811 (2006). https://doi.org/10.1016/j.nucengdes.2005.09.024